Combined Use of Anisotropic Silver Nanoprisms with Different Aspect Ratios for Multi-Mode Plasmon-Exciton Coupling

Naoto Takeshima[1], Kosuke Sugawa[1*] , Hironobu Tahara[2], Shota Jin[1], Masaki Noguchi[1], Yutaro Hayakawa[1], Yuhei Yamakawa[1] and Joe Otsuki[1]

Abstract

Absorption enhancement based on interaction between the localized surface plasmon (LSP) and molecular exciton is one of the most important phenomena for the development of high-performance solar devices. In this study, hybrids of plasmonic metal nanoparticles and dye molecules have been developed, which exhibit enhanced absorption at precisely tuned wavelengths in a visible region. The hybrids consist of a porphyrin derivative, which has four absorption peaks (Q-bands) in a range of 500–700 nm, and triangular silver nanoprisms (AgPRs), which are developed by us to exhibit precisely tuned LSP resonance wavelengths. Absorption enhancement over the whole Q-band range is induced by the combined use of three kinds of AgPRs of different aspect ratios. Furthermore, the quantitative evaluation of absorption enhancement based on the LSP-based fluorescence enhancement phenomenon has demonstrated that efficient absorption enhancement can be effected at multiple wavelengths.

Keywords: Localized surface plasmon, Tetraphenyl porphyrin, Fluorescence enhancement, Absorption enhancement, Silver nanoprisms, Plasmon-exciton interaction

Introduction

Controlling light-matter interaction is one of the intensively researched topics in the photochemical science [1]. The utilization of metal nanoparticles has been recognized as a way to strengthen the light-matter interaction because they generate strong electromagnetic fields at the nanoscale dimension upon excitation of the localized surface plasmon (LSP) resonance. In particular, the interaction between LSP and exciton of photofunctional molecules is attracting much attention because of the occurrence of various beneficial optical phenomena including a huge emission enhancement [2], suppression of photochemical quenching [3], plasmonic resonance energy transfer [4], enhanced water splitting [5], and so on. Antosiewicz et al. classified the interactions between metal nanoparticles and photofunctional molecules into three regimes according to the strength of interaction:

(1) the enhanced absorption regime, (2) the induced transparency regime, and (3) the strong coupling regime [6]. The strong coupling leads to the splitting of state in which the LSP and molecular exciton states are mixed, which is manifested in the splitting of the extinction peak at the wavelength of the molecular resonance. On the other hand, in the enhanced absorption regime, the absorption and scattering components of the LSP are damped, whereas the molecular absorption is increased by the energy transfer from the LSP to the molecule. The enhanced molecular absorption cancels the damped absorption component of LSP resonance but the uncompensated damped scattering component remains as a dip in the extinction spectrum. The induced transparency regime refers to an intermediate case between the absorption enhancement regime and the strong coupling regime. Among these, the absorption enhancement is quite important for the development of highly efficient solar devices [7–11]. Particularly, absorption enhancement over a wide range of wavelength is essential to utilize the wide solar spectrum. However, the multiwavelength generation of enhanced absorption through the

* Correspondence: sugawa.kosuke@nihon-u.ac.jp
[1]Department of Materials and Applied Chemistry, College of Science and Technology, Nihon University, Kanda-Surugadai, Chiyoda-ku, Tokyo 101-8308, Japan
Full list of author information is available at the end of the article

interaction between the LSP and the exciton has never been demonstrated. The generation of spectral dips at multiple wavelengths was reported, which was achieved by using plasmonic metal nanoparticles in combination with two different dye molecules, but this phenomenon was attributed to the Rabi oscillation in the strong coupling case and did not lead to absorption enhancement [12]. In another report on the plasmon-exciton coupling at multiple wavelengths using a combination of cyanine dye molecules exhibiting two absorption bands and metal nanorods [13], the absorption enhancement was not identified.

In this study, we have succeeded in enhancing light absorption at multiple wavelengths over a visible region through the interaction between the exciton of dye molecules and the LSP resonances of three different kinds of plasmonic metal nanoparticles. The achievement was made possible by developing a precise tuning technique of LSP wavelength of triangular silver nanoprisms (AgPRs). Furthermore, the enhancement factors of absorption were quantitatively evaluated utilizing the fluorescence enhancement, which occurred as a result of the interaction of exciton of dye molecules with the LSP resonance.

Method/Experimental
Materials
Milli-Q-grade water (resistivity: 18.2 MΩ cm) was used for the preparation of all aqueous solutions. Toluene was purchased from Kishida Chemical (Japan). 5,10,15,20-Tetraphenyl-21H,23H-porphyrin (TPP), sodium tetrahydroborate (NaBH$_4$), silver nitrate (AgNO$_3$), and polyethyleneimine (PEI) (MW ~ 10,000) were purchased from Fujifilm Wako Pure Chemical (Japan). Trisodium citrate dihydrate, sodium hydroxide (NaOH), ammonium solution (NH$_3$, 28%), and hydrogen peroxide solution (H$_2$O$_2$, 30%) were purchased from Kanto Chemical (Japan). All chemicals were used without further purification.

Measurements
Transmission electron microscopy (TEM) and atomic force microscopy (AFM, tapping mode) were carried out using a Hitachi HF-2000 microscope and a Hitachi SPI-3800N-SPA400 microscope, respectively. The extinction spectra of sample substrates were measured by a normal transmittance setup using a JASCO V-770 spectrometer. The absorption and scattering spectra were measured by the spectrometer (JASCO V-770) equipped with an integrating sphere according to a previous report [14]. Fluorescence excitation spectra of sample substrates were measured by a JASCO FP-8600 fluorescence spectrophotometer. The calculation for the extinction spectra of AgPRs was conducted using the boundary element method (BEM) with retarded electromagnetic fields for the full Maxwell equations [15]. To produce the random orientation of the AgPRs in solution phase, the transmission spectra were averaged over all allowed combinations of incident light polarization (E_x, E_y, E_z) and incident light propagation orientations (k_x, k_y, k_z). The geometry models are shown in Additional file 1: Figure S1. The dielectric function of silver was taken from the previous report by Rakic et al. [16].

Synthesis of AgPRs with Different Resonance Wavelengths
The AgPRs with precisely tuned resonance wavelengths of the in-plane dipole mode (500, 540, 560, 625, 645, and 675 nm) were synthesized by the light-mediated method developed by us. An aqueous solution (100 mL) containing trisodium citrate (5 mM) as a protective agent and NaBH$_4$ (0.2 mM) as a reducing agent was injected into an aqueous solution (100 mL) of AgNO$_3$ (1 mM) in an ice bath under stirring. The mixture was further stirred for 1 h, leading to the formation of Ag nanospheres with an average diameter of 11 nm. After an aqueous solution of NaOH (0.2 M, 100 μL) was injected into the colloidal solution of Ag nanospheres (10 mL) to adjust the pH to 11.2, light-emitting diode (LED) light was irradiated, which led to the formation of AgPRs. Specifically, the resonance wavelength of in-plane dipole mode of AgPRs was precisely adjusted by sequential irradiation of LED light with different wavelengths of 470 ± 5 nm (5800 mcd, 3 × 3 arrays), 525 ± 5 nm (18,000 mcd, 3 × 3 arrays), and 590 ± 5 nm (50,000 mcd, 3 × 3 arrays) for predetermined periods of time as summarized in Table 1, whereas the irradiation setup is shown in

Table 1 Synthetic conditions for AgPRs with various resonance wavelengths

1: Irradiation period of 470 nm/h	2: Irradiation period of 525 nm/h	3: Irradiation period of 590 nm/h	Resonance wavelength[a] of AgPRs/nm
24	0	0	500 ± 2.0
4	20	0	540 ± 1.2
2	22	0	560 ± 0.6
0	6	42	625 ± 3.5
0	3	45	645 ± 5.0
0	2	46	675 ± 1.7

[a]Mean values and standard deviations

Additional file 1: Figure S2. The obtained AgPRs are designated as AgPRs-*X*, in which *X* indicates the resonance wavelength.

### Preparation of Hybrids of TPP and AgPRs

To clean the surface, a glass substrate (1.5×2.0 cm^2) was immersed into a mixed aqueous solution of 30% H_2O_2 and 28% NH_3 (1/1 = V/V) at 100 °C for 3 h, followed by washing with Milli-Q water. The cleaned substrate was kept in Milli-Q water until use. The substrate was modified with positively-charged PEI by immersing it into an aqueous solution of PEI (4.2 mg/mL) for 1 min, followed by washing with Milli-Q water. The positively charged substrate was then immersed in the colloidal solution to electrostatically immobilize AgPRs, which were negatively charged owing to the citric acid sheath. The immersion was continued until the extinction intensity of the main LSP resonance band (in-plane dipole mode) reached 0.2; thus obtained substrate is referred to as AgPRs-*X*/glass. The extinction intensity of the LSP of AgPRs on the glass plate was set to be 0.2 to avoid the LSP coupling between adjacent AgPRs observed for denser samples [17]. For the preparation of a glass plate on which three AgPRs (LSP resonance wavelengths of 500, 560, and 645 nm) were immobilized (AgPRs-ternary/glass), the positively charged glass plate was immersed sequentially into respective colloidal solutions of AgPRs until each extinction intensity of the main LSP resonance reached 0.1. A toluene solution of TPP (1.5 mM) was spin-coated (3000 rpm, 30 s) on AgPRs-*X*/glass and AgPRs-ternary/glass, affording the hybrids of TPP and AgPRs (TPP/AgPRs-*X* and TPP/AgPRs-ternary). TPP was also deposited on a bare glass substrate as a reference by spin-coating the TPP solution onto the PEI-modified glass substrate (TPP/glass).

Results and Discussion

Optical Properties of TPP and Optical Properties and Morphologies of AgPRs

In this study, a porphyrin derivative, TPP (molecular structure: Fig. 1a), was employed as a photofunctional
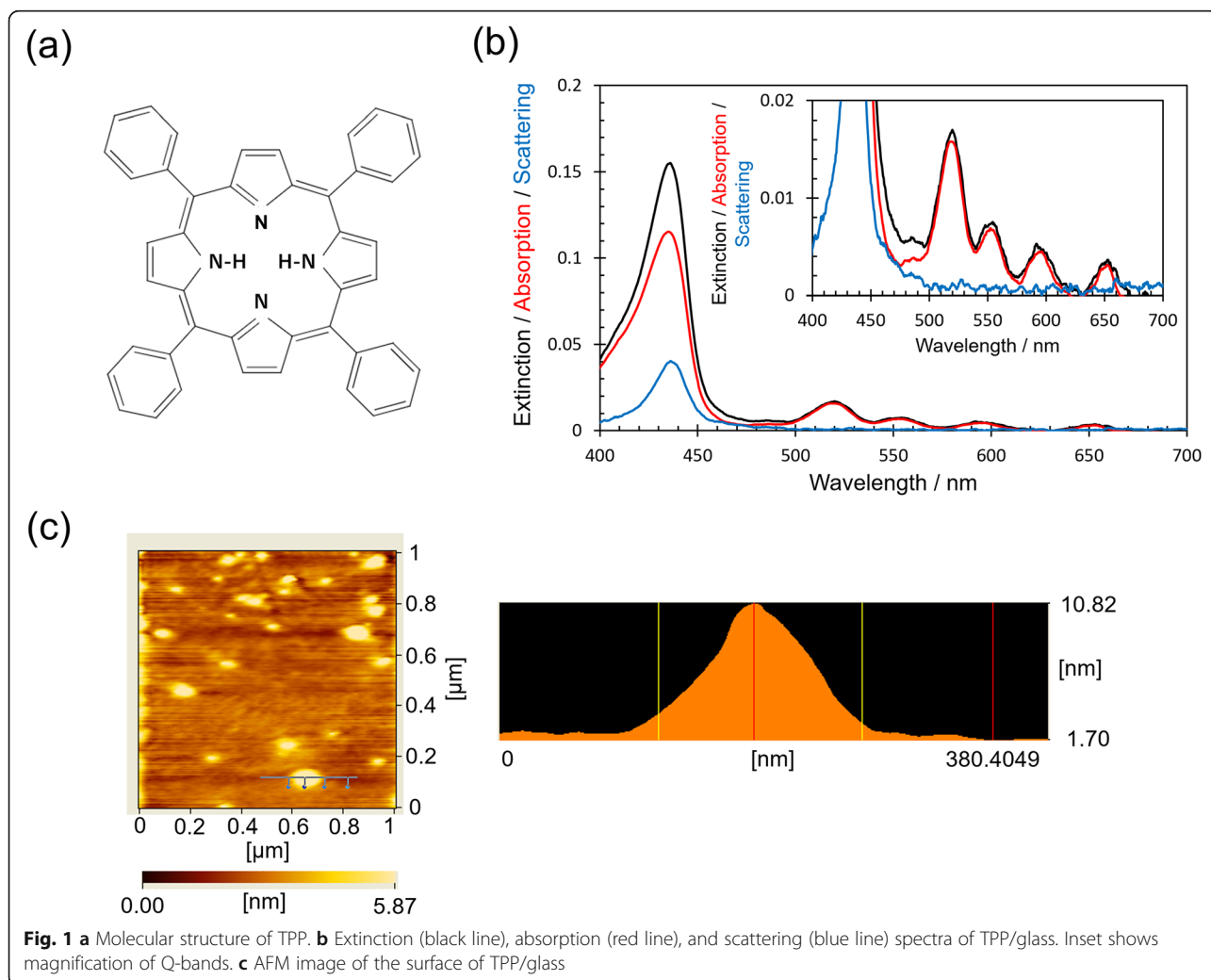


Fig. 1 a Molecular structure of TPP. **b** Extinction (black line), absorption (red line), and scattering (blue line) spectra of TPP/glass. Inset shows magnification of Q-bands. **c** AFM image of the surface of TPP/glass

molecule. Porphyrins, synthetic analogues of natural chlorophylls, are frequently used as light harvester owing to their wide absorption in the visible region [18]. However, the absorption coefficients of four absorption peaks in 500–700 nm region are relatively low (Q-bands, absorption coefficient: $\sim 10^4$ M^{-1} cm^{-1}), whereas the absorption around 420 nm is quite strong (Soret band, absorption coefficient: $> 10^5$ M^{-1} cm^{-1}). Therefore, we set out an attempt to enhance the absorption of Q-bands by means of the LSP of metal nanoparticles. Figure 1b shows the extinction, absorption, and scattering spectra of TPP/glass. An extinction peak of the Soret band at 435 nm and four extinction peaks of the Q-bands at 519, 552, 596, and 653 nm [19] were observed. Compared to the peak wavelengths of Q-bands in a toluene solution of TPP (514, 548, 591, and 649 nm, Additional file 1: Figure S3), those of the TPP/glass were slightly red-shifted. Also, the extinction at the Soret band was accompanied by a prominent scattering component. These results suggest that the TPP molecules densely aggregated on the glass substrate because the scattering cross section of molecular aggregates is proportional to the square of the volume of the aggregates and the red-shift can be attributed to the π-π interaction of TPP [20]. To investigate the morphology of the molecular aggregates, the AFM measurement was conducted for TPP/glass. As shown in Fig. 1c, the glass surface was scattered with the molecular aggregates having a height of 7 ± 2 nm and a diameter of 108 ± 29 nm.

A large-scale, reproducible synthesis of plasmonic metal nanoparticles which generate strong LSP resonance at precisely tuned wavelengths is highly desired for a large-scale applications. Absorption enhancement of the Q-bands of porphyrins spread over a macroscopic substrate is a model case for such applications, which we will describe in this work. A satisfactory technique of metal nanoparticle preparation that meets the demand has been rarely reported [21, 22].

We have succeeded in synthesizing AgPRs which can generate strong local electromagnetic fields at precisely tuned LSP resonance wavelengths in sufficient amount [17, 23]. The wavelength region in which the LSP resonance occurs matches the Q-band region of porphyrins. Our method is based on the light-mediated method, which was originally developed by Mirkin's research group [24, 25]. In the preparation, the AgPRs are synthesized by the irradiation of light to citrate-stabilized Ag nanospheres with a diameter below 10 nm. Hot electrons and holes are formed during the decay of the LSP resonance upon light irradiation. While the hot holes are transferred to citric acid adsorbed on the Ag surfaces, the hot electrons reduce silver ions, resulting in the formation of AgPRs. Although the LSP resonance wavelength was controlled by choosing the excitation light

wavelength to a certain degree, the precise tuning has never been achieved by a single excitation wavelength in the previous reports [25–27]. In this study, we have succeeded in preparing AgPRs exhibiting the LSP resonance wavelengths with an unprecedented precision. This was achieved by tuning the sequence, wavelengths, and duration of irradiation (see experimental section and Table 1) in the process of converting the Ag nanospheres into AgPRs. For example, irradiation of 470 nm light alone produced AgPRs exhibiting the LSP resonance at 500 nm. Irradiation of 470 nm light followed by 525 nm light (keeping the total irradiation time unchanged) produced AgPRs with a red-shifted LSP resonance. During the first irradiation process of the 470 nm light, small AgPRs were formed by oriented attachment-like two-dimensional coalescence of Ag nanospheres. In the second 525 nm light irradiation, the AgPRs grew in an Ostwald ripening process to a specific size at the consumption of the remaining Ag nanospheres. Thus, obtained AgPRs generated the LSP resonance at exact wavelengths of 500, 540, 560, 625, 645, and 675 nm with small standard deviations (0.6–5 nm, see Table 1) under our specific conditions. The extinction spectra of respective colloidal solutions of AgPRs prepared five times are shown in Additional file 1: Figure S4, which clearly indicates that our synthetic method has a remarkable reproducibility in generating LSP resonances at exact wavelengths. Normalized extinction spectra and a photograph of the colloidal aqueous solutions of the obtained AgPRs are shown in Fig. 2a, b, respectively. All the AgPRs showed a prominent resonance band within 500–700 nm. It was found by comparing the LSP wavelengths and the TEM images, which are shown in Fig. 2c, that the resonance band was red-shifted with increasing the edge length (AgPRs-500: 25 ± 3 nm, AgPRs-540: 30 ± 4 nm, AgPRs-560: 33 ± 5 nm, AgPRs-625: 44 ± 9 nm, AgPRs-645: 47 ± 10 nm, and AgPRs-675: 52 ± 7 nm). Since the thicknesses of AgPRs which are synthesized by the photochemical method are almost constant at *ca.* 10 nm regardless of their edge lengths [28], the difference in the resonance wavelengths can be attributed to the difference in the aspect ratio (the ratio of edge length to thickness) [29]. To prove the correlation between the LSP wavelength and its aspect ratio, we calculated the extinction spectra using the BEM for AgPRs having the experimentally obtained edge lengths and a fixed thickness of 10 nm which were surrounded by aqueous phase (refractive index: 1.333) (Fig. 2a). The calculated resonance wavelengths agreed very well with the experimentally obtained wavelengths (Fig. 2d), which indicated that the accurate control of resonance band of AgPRs was achieved by precisely controlling the aspect ratio. The experimental extinction spectra of AgPRs were somewhat broader than the calculated ones. This may be
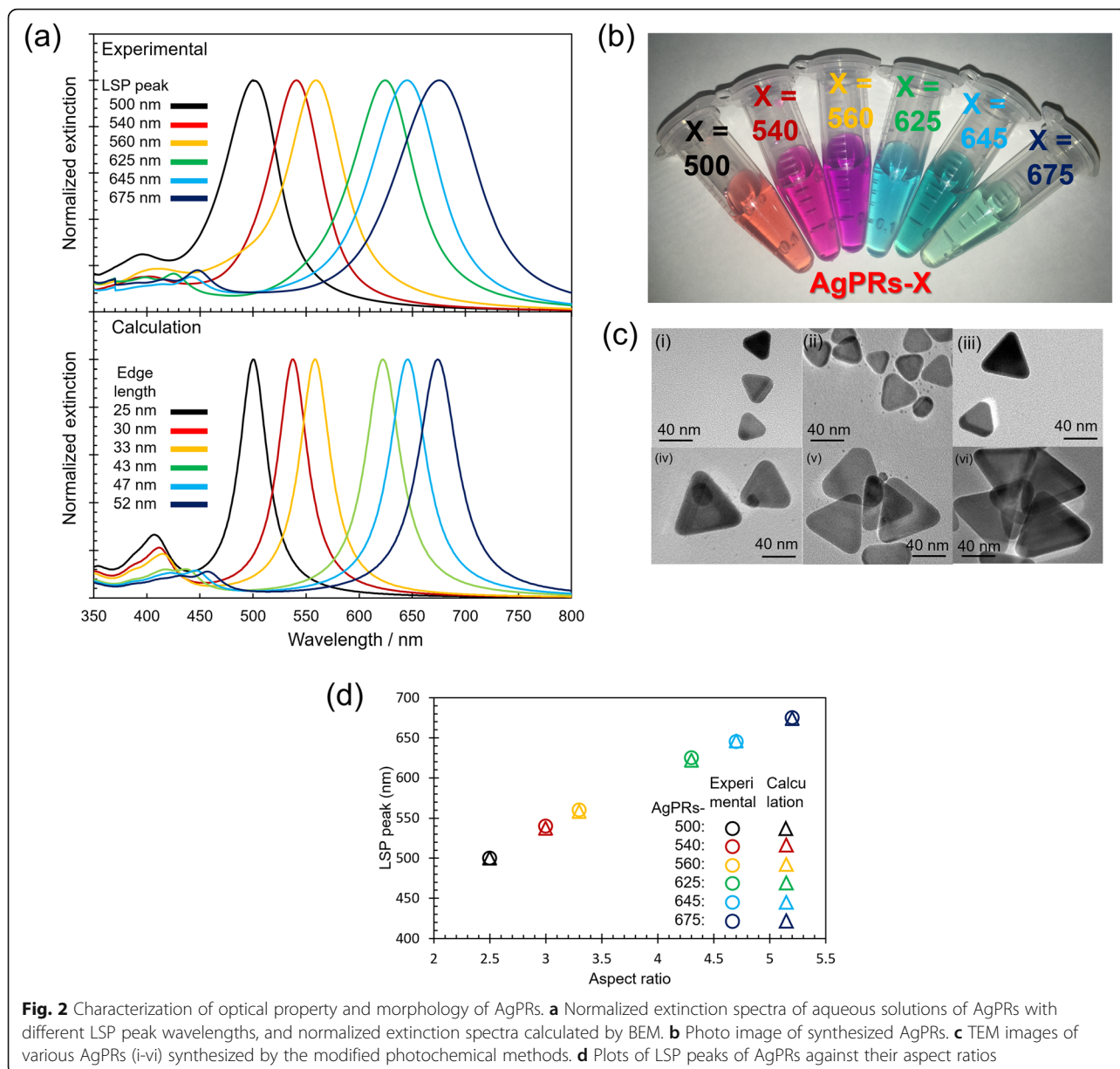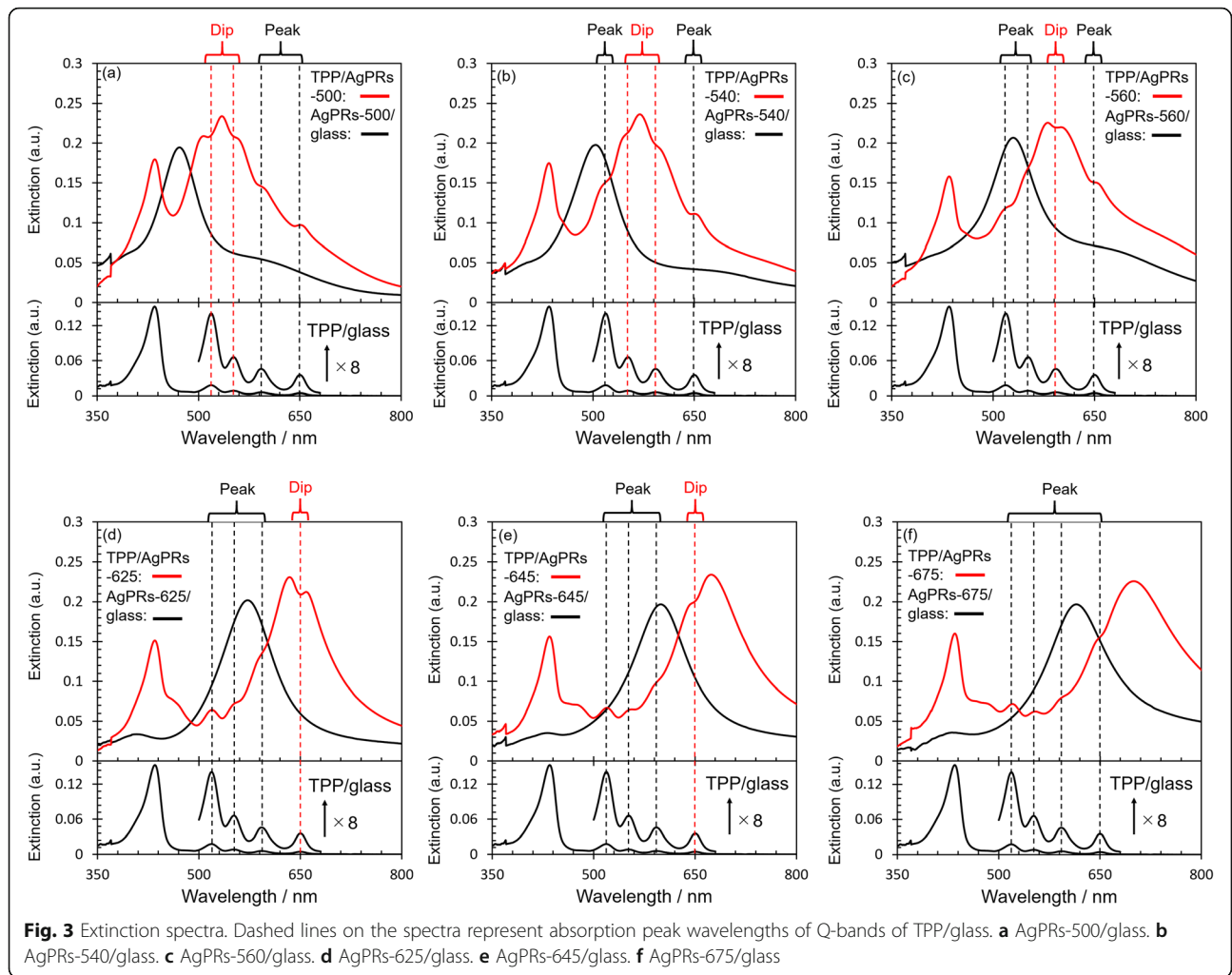
Fig. 2 Characterization of optical property and morphology of AgPRs. **a** Normalized extinction spectra of aqueous solutions of AgPRs with different LSP peak wavelengths, and normalized extinction spectra calculated by BEM. **b** Photo image of synthesized AgPRs. **c** TEM images of various AgPRs (i-vi) synthesized by the modified photochemical methods. **d** Plots of LSP peaks of AgPRs against their aspect ratios

partly because there was a distribution in the aspect ratios, albeit narrow, in the prepared AgPRs and partly because the solvent molecules (water) caused the chemical interface damping [30], both of which were not included in the calculations.

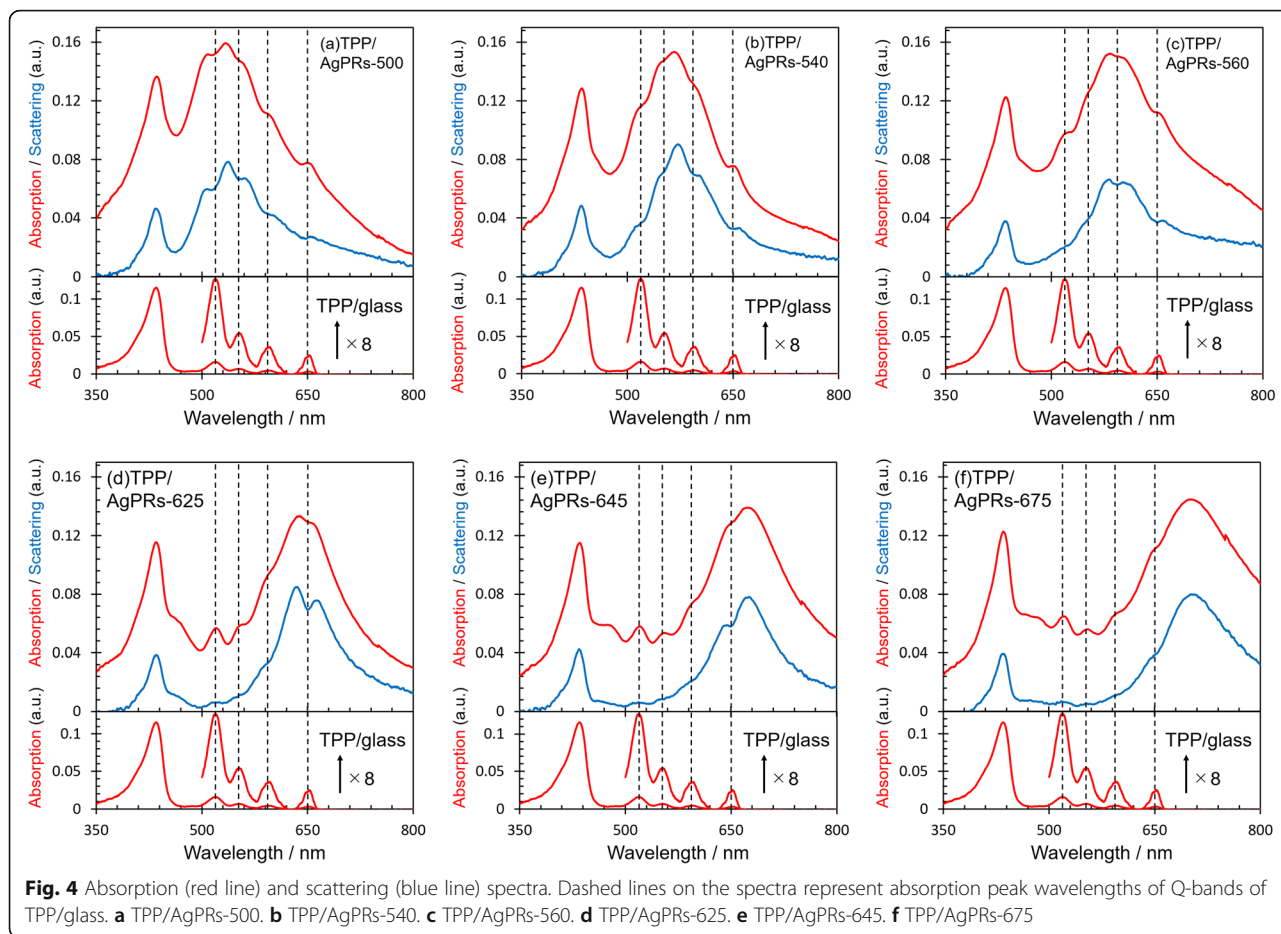### Interaction Between LSP of AgPRs and Exciton of TPP

To evaluate the interaction between the LSP of AgPRs and the exciton of TPP in TPP/AgPRs-*X*, the extinction spectra were measured for TPP/glass (as a reference), AgPRs/glass, and TPP/AgPRs-*X* (Fig. 3). The dashed lines in Fig. 3 indicate the peak wavelengths of Q-bands observed on TPP/glass. The resonance wavelengths of the in-plane dipole mode for all AgPRs/glass were blue-

shifted by several tens of nanometers as compared with those in an aqueous phase (Fig. 2a). These shifts are attributed to a change in the refractive index of the medium surrounding the AgPRs from the aqueous phase to air (refractive index: 1.000) [31–33]. After spin-coating the TPP solution onto AgPRs-*X*/glass, the Soret band was observed at 436 nm. In addition, the LSP resonance bands were red-shifted, resulting in the LSP band within 500–700 nm for all AgPRs. These results suggest that the AgPRs were covered with TPP aggregates because the refractive index (approximately 1.6) of TPP is larger than that of air [18]. Note that prominent peaks or dips were observed at the wavelengths of the Q-band peaks on the LSP resonance band for all TPP/

Fig. 3 Extinction spectra. Dashed lines on the spectra represent absorption peak wavelengths of Q-bands of TPP/glass. **a** AgPRs-500/glass. **b** AgPRs-540/glass. **c** AgPRs-560/glass. **d** AgPRs-625/glass. **e** AgPRs-645/glass. **f** AgPRs-675/glass

AgPRs-*X*. For example, in the case of TPP/AgPRs-500, while spectral dips were observed at 515 and 552 nm where the LSP resonance was strongly excited, peaks were observed at 595 and 654 nm in the edge region of the LSP resonance band. The latter positions are in the peripheral region of the LSP band where the electromagnetic field around the AgPRs is weak. Therefore, the coupling between the LSP resonance and the TPP exciton is weak, resulting in the overall spectrum resembling the sum of individual spectra. On the other hand, only peaks were observed for TPP/AgPRs-675 because the Q-bands overlap only with the peripheral region of the LSP band (Fig. 3f), suggesting inefficient interaction between the LSP and the exciton [34]. We emphasize based on these data that the strong interaction between the LSP and exciton, which is manifested by the appearance of dips, is efficiently induced only at a narrow wavelength region where the LSP resonance is strongly excited. Therefore, the combined use of multiple AgPRs with the LSP resonance at multiple wavelengths over the Q-band region is required.

In the case classified as the absorption enhancement, which represents a weak coupling case, light absorption attributed to the exciton generation increases, whereas the extinction of LSP at the same wavelength decreases. As a result, the total absorption component changes little because the absorption enhancement to generate excitons is canceled out by the absorption decrease in the LSP band. On the other hand, the net scattering component decreases, resulting in a dip in the total extinction spectrum [6]. In the case of the strong coupling, prominent dips are observed similarly in both absorption and scattering spectra because two hybrid states separated in energy are formed in place of independent eigenstates. The induced transparency refers an intermediate case between the absorption enhancement and the strong coupling [6, 35, 36]. To further clarify the strength of interaction between the LSP and the exciton in our hybrids, the absorption and scattering spectra of TPP/AgPRs-*X* were measured (Fig. 4) [6, 37, 38]. Although prominent dips were observed in the region where the LSP was strongly excited in the scattering spectra for all

Fig. 4 Absorption (red line) and scattering (blue line) spectra. Dashed lines on the spectra represent absorption peak wavelengths of Q-bands of TPP/glass. **a** TPP/AgPRs-500. **b** TPP/AgPRs-540. **c** TPP/AgPRs-560. **d** TPP/AgPRs-625. **e** TPP/AgPRs-645. **f** TPP/AgPRs-675

TPP/AgPRs-*X* except for TPP/AgPRs-675, the dips were less prominent in the corresponding absorption spectra. These observations suggested that our hybrids TPP/AgPRs-500, 540, 560, 625, and 645 were in the regime of absorption enhancement with respect to the coupling strength.
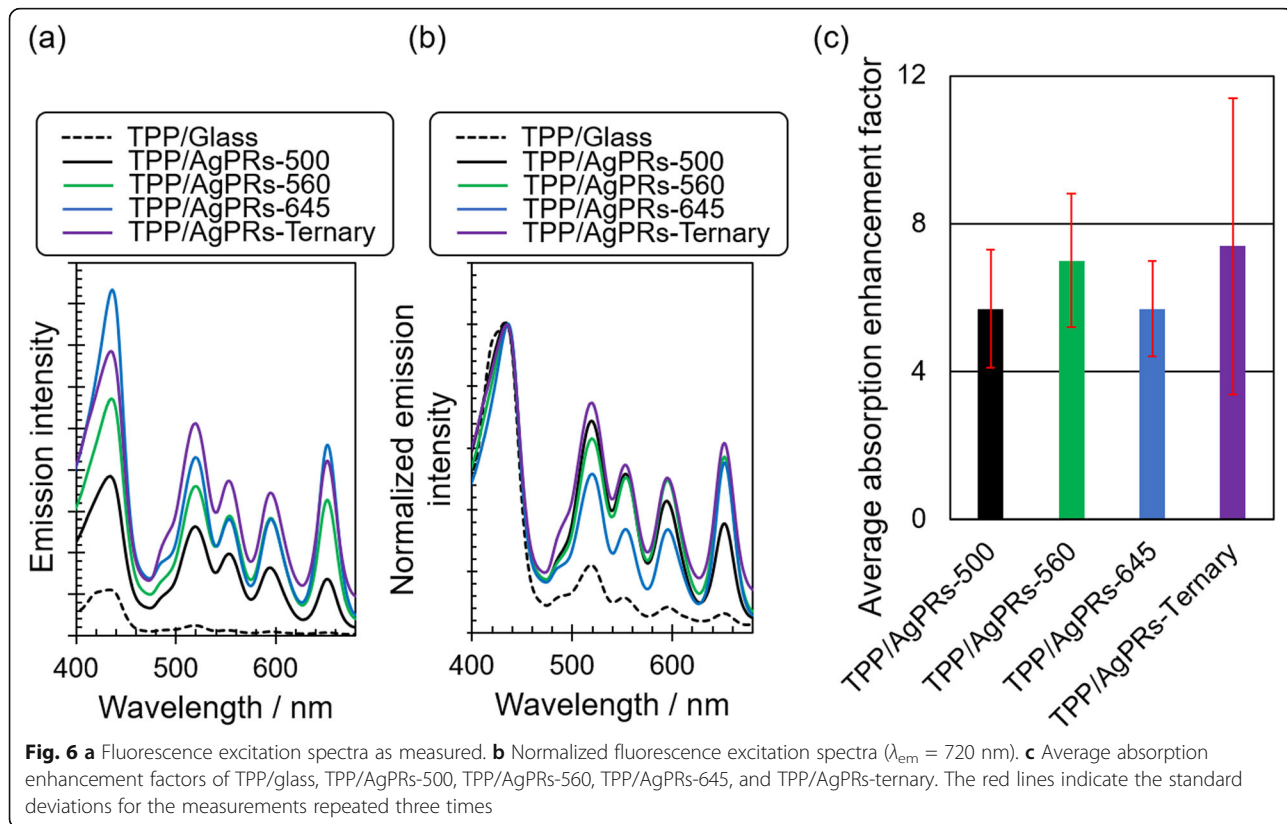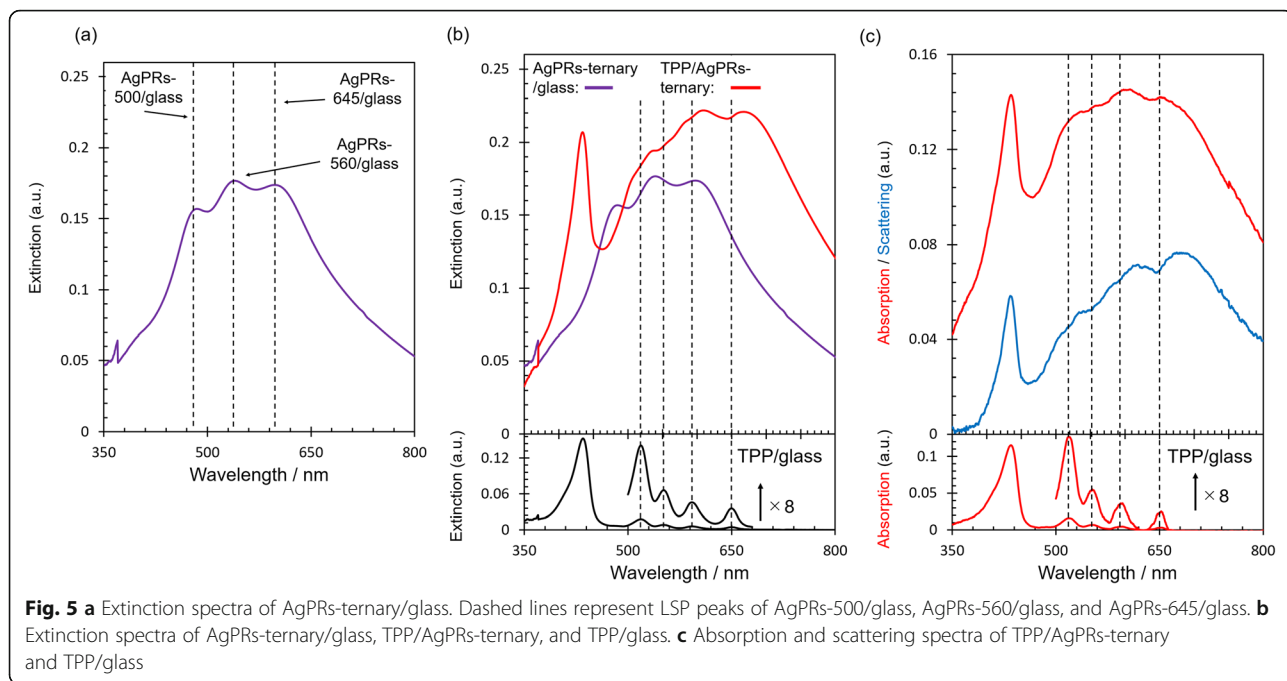
Realization of Enhanced Absorption Over the Whole Q-Bands

Although we have succeeded in achieving the absorption enhancement at the region where the LSP resonance is strongly excited, absorption enhancement over a wider range covering the whole Q-bands may be beneficial in terms of solar light utilization. To achieve this, we hybridized TPP and AgPRs-ternary/glass (denoted as TPP/AgPRs-ternary). The extinction spectrum of AgPRs-ternary/glass is shown in Fig. 5a. Three distinct bands were observed at 485, 540, and 598 nm, which were assigned to the LSP resonance bands of AgPRs-500, 560, and 645, respectively. The extinction spectrum of TPP/AgPRs-ternary, which is shown in Fig. 5b, exhibited four dips at the wavelengths corresponding to the Q-band peaks. Furthermore, as shown in Fig. 5c, while the

prominent four dips were observed at the Q-band wavelengths in the scattering spectrum, these dips did not appear in the absorption spectrum. These results suggested that the strength of interaction between the LSPs of AgPRs-500, 560, and 645 and the excitons generated in the whole Q-band wavelengths was in the enhanced absorption regime.

Effect of Absorption Enhancement on Photodynamics of TPP

To quantitatively investigate the effect of the absorption enhancement on the photodynamics of TPP, the fluorescence excitation spectra of TPP/AgPRs-500, 560, 645, and ternary (λ_{em} = 720 nm) were measured (Fig. 6a). The fluorescence radiation of these hybrids was significantly enhanced by excitation in the region of both the Soret and Q-bands as compared to that of TPP/glass. The fluorescence enhancement factors at the Q-band peaks were in the range of 11–71 (see Additional file 1: Figure S5a). The fluorescence enhancement owing to the LSP resonance can be attributed to two mechanisms: the photoexcitation enhancement (i.e., absorption enhancement), which is induced when the LSP resonance band

Fig. 5 a Extinction spectra of AgPRs-ternary/glass. Dashed lines represent LSP peaks of AgPRs-500/glass, AgPRs-560/glass, and AgPRs-645/glass. **b** Extinction spectra of AgPRs-ternary/glass, TPP/AgPRs-ternary, and TPP/glass. **c** Absorption and scattering spectra of TPP/AgPRs-ternary and TPP/glass

Fig. 6 a Fluorescence excitation spectra as measured. **b** Normalized fluorescence excitation spectra (λ_{em} = 720 nm). **c** Average absorption enhancement factors of TPP/glass, TPP/AgPRs-500, TPP/AgPRs-560, TPP/AgPRs-645, and TPP/AgPRs-ternary. The red lines indicate the standard deviations for the measurements repeated three times

overlaps with the photoexcitation wavelength, and the acceleration in radiative decay rate, which is induced when the LSP resonance band overlaps with the fluorescence wavelength. The fluorescence enhancement for the Q-bands excitation could be induced by both of these mechanisms because the photoexcitation and fluorescence wavelengths overlap with the LSP resonance bands of TPP/AgPRs-500, 560, 645, and ternary. On the other hand, the fluorescence was also enhanced by 2.9–6.4 times for the Soret band excitation (see Additional file 1: Figure S5a). It is likely that the enhancement is solely attributed to the acceleration in the radiative decay rate because the excitation wavelength is separated far from the main LSP resonance bands of AgPRs in this case. Thus, the fluorescence enhancement factors were calculated using the fluorescence excitation spectra normalized at the Soret band (435 nm, Fig. 6b), which can be attributed to the net absorption enhancement. The average enhancement factors for the Q-bands are shown in Fig. 6c, obtained by averaging enhancement factors for respective Q-band peaks (Additional file 1: Figure S5b). Consequently, TPP/AgPRs-ternary showed the absorption enhancement uniformly at all the Q-band peaks resulting in the enhancement factor of 7.4. This result indicated that the absorption enhancement based on plasmon-exciton coupling was achieved over the broad wavelength region by combined use of AgPRs with different aspect ratios, which points to the usefulness of our precise tuning technique of LSP wavelengths. Randomly distributed polydisperse AgPRs would also enhance a wide range of absorption but many molecules would be placed out of resonance with AgPRs. Combining AgPRs of which the LSP resonance wavelength is precisely tuned to the molecular absorption peak positions would be the most efficient strategy in harvesting a spectrum of light. Thus, our precise tuning technique is promising for the development of high-performance solar devices.

Conclusion

We have succeeded in synthesizing AgPRs with well-defined resonance wavelengths, which can be precisely tuned over a wide visible region. The difference in resonance wavelengths is attributed to the difference in their aspect ratios. The combined use of AgPRs with three different aspect ratios led to the absorption enhancement over the whole Q-bands, which was demonstrated by their extinction, absorption, and scattering spectra. In addition, absorption enhancement factors were quantitatively evaluated from the fluorescence excitation spectra, which demonstrated the usefulness of our protocol to produce AgPRs exhibiting precisely tuned LSP resonance wavelengths in realizing absorption enhancement over the wide visible wavelength region.

Thus, the combined use of AgPRs with different aspect ratios have a great potential for enhancing light-matter interaction in a wide wavelength region, which paves the way for the fabrication of high-performance optoelectronic devices including solar cells, photocatalysts, and bio-imaging sensors.

Supplementary information

Supplementary information accompanies this paper at https://doi.org/10.1186/s11671-020-3248-8.

Additional file 1: Figure S1. Geometric models of AgPRs with various LSP resonance wavelengths. **Figure S2.** A Setup for the irradiation of LED light to a colloidal aqueous solution of Ag nanospheres. **Figure S3.** Normalized extinction and emission spectra of a toluene solution of TPP (1×10^{-6} M). **Figure S4.** Extinction spectra of colloidal aqueous solutions of AgPRs synthesized five times. **Figure S5.** (a) Enhancement factor of fluorescence obtained from fluorescence excitation spectra for TPP/AgPRs-500, TPP/AgPRs-560, TPP/AgPRs-645, and TPP-ternary (λ_{em} = 720 nm) at (i) 435 nm, (ii) 519 nm, (iii) 552 nm, (iv) 596 nm, and (v) 653 nm, respectively. (b) Absorption enhancement at the respective Q-band wavelengths.

Abbreviations
AFM: Atomic force microscopy; AgNO$_3$: Silver nitrate; AgPRs: Silver nanoprisms; BEM: Boundary element method; H$_2$O$_2$: Hydrogen peroxide; IT: Induced transparency; LED: Light-emitting diode; LSP: Localized surface plasmon; NaBH$_4$: Sodium tetrahydroborate; NaOH: Sodium hydroxide; NH$_3$: Ammonia; PEI: Polyethyleneimine; TEM: Transmission electron microscopy; TPP: Tetraphenylporphyrin

Acknowledgments
Not applicable.

Authors' Contributions
All authors read and approved the final manuscript.

Availability of Data and Materials
All data generated or analyzed during this study are included in this published article and its supplementary information files.

Competing Interests
The authors declare that they have no competing interests.

Author details
[1]Department of Materials and Applied Chemistry, College of Science and Technology, Nihon University, Kanda-Surugadai, Chiyoda-ku, Tokyo 101-8308, Japan. [2]Graduate School of Engineering, Nagasaki University, Bunkyo, Nagasaki 852-8521, Japan.

References
1. Li X, Zhou L, Hao Z, Wang QQ (2018) Plasmon-exciton coupling in complex systems. Adv Opt Mater 6:1800275. https://doi.org/10.1002/adom.201800275
2. Sun J, Hu H, Zheng D, Zhang D, Deng Q, Zhang S, Xu H (2018) Light-emitting plexciton: exploiting plasmon-exciton interaction in the intermediate coupling regime. ACS Nano 12(10):10393–10402. https://doi.org/10.1021/acsnano.8b05880
3. Munkhbat B, Wersall M, Baranov DG, Antosiewicz TJ, Shegai T (2018) Suppression of photo-oxidation of organic chromophores by strong coupling to plasmonic nanoantennas. Sci Adv 4(7):eaas9552. https://doi.org/10.1126/sciadv.aas9552

4. Gao MX, Zou HY, Li YF, Huang CZ (2017) General sensitive detecting strategy of ions through plasmonic resonance energy transfer from gold nanoparticles to rhodamine spirolactam. Anal Chem 89(3):1808–1814. https://doi.org/10.1021/acs.analchem.6b04124

5. Shi X, Ueno K, Oshikiri T, Sun Q, Sasaki K, Misawa H (2018) Enhanced water splitting under modal strong coupling conditions. Nat Nanotechnol 13:953-958. doi. 10.1038/s41565-018-0208-x

6. Antosiewicz TJ, Apell SP, Shegai T (2014) Plasmon-exciton interactions in a core-shell geometry: from enhanced absorption to strong coupling. ACS Photonics 1(5):454–463. https://doi.org/10.1021/ph500032d

7. Kim GM, Tatsuma T (2017) Photocurrent enhancement of perovskite solar cells at the absorption edge by electrode-coupled plasmons of silver nanocubes. J Phys Chem C 121(21):11693–11699. https://doi.org/10.1021/acs.jpcc.7b02799

8. Cushing SK, Li J, Meng F, Senty TR, Suri S, Zhi M, Li M, Bristow AD, Wu N (2012) Photocatalytic activity enhanced by plasmonic resonant energy transfer from metal to semiconductor. J Am Chem Soc 134(36):15033–15041. https://doi.org/10.1021/ja305603t

9. Cai Y, Wang Z, Yan S, Ye L, Zhu J (2018) Ultraviolet absorption band engineering of graphene by integrated plasmonic structures. Opt Mater Express 8(11):3295–3306. https://doi.org/10.1364/OME.8.003295

10. Liu T, Jiang X, Zhou C, Xiao S (2019) Black phosphorus-based anisotropic absorption structure in the mid-infrared. Opt Express 27(20):27619–27627. https://doi.org/10.1364/OE.27.027618

11. Cai Y, Zhu J, Liu QH (2015) Tunable enhanced optical absorption of graphene using plasmonic perfect absorbers. Appl Phys Lett 106(4):043105–043101. https://doi.org/10.1063/1.4906996

12. Melnikau D, Govyadinov AA, Sanchez-Iglesias A, Grzelczak M, Nabiev IR, Liz-marzan LM, Rakovich YP (2019) Double Rabi splitting in a strongly coupled system of core-shell Au@Ag nanorods and J-aggregates of multiple fluorophores. J Phys Chem Lett 10(20):6137–6143. https://doi.org/10.1021/acs.jpclett.9b01988

13. Zhang YF, Yang DJ, Wang JH, Wang YL, Ding SJ, Zhou L, Hua Hao Z, Wang QQ (2015) Multiple hybridized resonance of IR-806 chromonic molecules strongly coupled to Au nanorods. Nanoscale 7:8503–8509. https://doi.org/10.1039/C5NR00051C

14. Stete F, Koopaman W, Bargheer M (2017) Signatures of strong coupling on nanoparticles: revealing absorption anticrossing by tuning the dielectric environment. ACS Photonics 4(7):1669–1676. https://doi.org/10.1021/acsphotonics.7b00113

15. Waxenegger J, Trugler A, Hohenester U (2015) Plasmonic simulations with the MNPBEM toolbox: consideration of substrates and layer structures. Comput Phys Commun 193:138–150. https://doi.org/10.1016/j.cpc.2015.03.023

16. Rakic AD, Djurisic AB, Elazar JM, Majewski ML (1998) Optical properties of metallic films for vertical-cavity optoelectronic devices. Appl Opt 37(22):5271–5283. https://doi.org/10.1364/AO.37.005271

17. Jin S, Sugawa K, Takeshima N, Tahara H, Igari S, Yoshinari S, Kurihara Y, Watanabe S, Enoki M, Sato K, Inoue W, Tokuda K, Akiyama T, Katoh R, Takase K, Ozawa H, Okazaki T, Watanabe T, Otsuki J (2018) Precise control of localized surface plasmon wavelength is needed for effective enhancement of triplet-triplet annihilation-based upconversion emission. ACS Photonics 5(12):5025–5037. https://doi.org/10.1021/acsphotonics.8b01292

18. Otsuki J (2018) Supramolecular approach towards light-harvesting materials based on porphyrins and chlorophylls. J Mater Chem A 9:6710–6753. https://doi.org/10.1039/C7TA11274B

19. Tuerdi G, Nizamidin P, Kari N, Yimit A, Wang F (2018) Optochemical properties of gas-phase protonated tetraphenylporphyrin investigated using an optical waveguide NH_3 sensor. RSC Adv 8:5614–5621. https://doi.org/10.1039/c7ra11643h

20. Pasternack RF, Collings PJ (1995) Resonance light scattering: a new technique for studying chromophore aggregation. Science 269(5226):935–939. https://doi.org/10.1126/science.7638615

21. Melnikau D, Esteban R, Savateeva D, Sanchez-Iglesias A, Grzelczak M, Schmidt MK, Liz-Marzan LM, Aizpurua J, Rakovich YP (2016) Rabi splitting in photoluminescence spectra of hybrid systems of gold nanorods and J-aggregates. J Phys Chem Lett 7(2):354–362. https://doi.org/10.1021/acs.jpclett.5b02512

22. Ni W, Yang Z, Chen H, Li L, Wang J (2008) Coupling between molecular and plasmonic resonances in freestanding dye-gold nanorod hybrid nanostructures. J Am Chem Soc 130(21):6692–6693. https://doi.org/10.1021/ja8012374

23. Takeshima N, Sugawa K, Tahara H, Jin S, Wakui H, Fukushima M, Tokuda K, Igari S, Kanakubo K, Hayakawa Y, Katoh R, Takase K, Otsuki J (2019) Plasmonic silver nanoprism-induced emissive mode control between fluorescence and phosphorescence of a phosphorescent palladium porphyrin derivative. ACS Nano 13(11):13244–13256. https://doi.org/10.1021/acsnano.9b06269

24. Jin R, Cao Y, Mirkin CA, Kelly KL, Schatz GC, Zheng JG (2001) Photoinduced conversion of silver nanospheres to nanoprisms. Science 294(5548):1901–1903. https://doi.org/10.1126/science.1066541

25. Jin R, Cao YC, Hao E, Metraux GS, Schatz GC, Mirkin CA (2003) Controlling anisotropic nanoparticle growth through plasmon excitation. Nature 425:487–490. https://doi.org/10.1038/nature02020

26. Lee GP, Shi Y, Lavoie E, Daeneke T, Reineck P, Cappel UB, Huang DM, Bach U (2013) Light-driven transformation processes of anisotropic silver nanoparticles. ACS Nano 7(7):5911–5921. https://doi.org/10.1021/nn4013059

27. Stamplecoskie KG, Scaiano JC (2010) Light emitting diode irradiation can control the morphology and optical properties of silver nanoparticles. J Am Chem Soc 132(6):1825–1827. https://doi.org/10.1021/ja910010b

28. Sugawa K, Takeshima N, Uchida K, Tahara H, Jin S, Tsunenari N, Akiyama T, Kusaka Y, Fukuda N, Ushijima H, Tsuchido Y, Hashimoto T, Hayashita T, Otsuki J (2015) Photocurrent enhancement of porphyrin molecules over a wide-wavelength region based on combined use of silver nanoprisms with different aspect ratios. J Mater Chem C 3:11439–11448. https://doi.org/10.1039/C5TC02606G

29. Zhang Q, Li N, Goebl J, Lu Z, Yin Y (2011) A systematic study of the synthesis of silver nanoplates: is citrate a "magic" reagent? J Am Chem Soc 133(46):18931–18939. https://doi.org/10.1021/ja2080345

30. Douglas-Gallardo OA, Berdakin M, Sanchez CG (2016) Atomistic insights into chemical interface damping of surface plasmon excitations in silver nanoclusters. J Phys Chem C 120(42):24389–24399. https://doi.org/10.1021/acs.jpcc.6b08519

31. Underwood S, Mulvaney P (1994) Effect of the solution refractive index on the color of gold colloids. Langmuir 10(10):3427–3430. https://doi.org/10.1021/la00022a011

32. Anker JN, Hall WP, Lyandres O, Shah NC, Zhao J, Van Duyne RP (2008) Biosensing with plasmonic nanosensors. Nat Mater 7(6):442–453. https://doi.org/10.1038/nmat2162

33. Mahmoud MA, Tabor CE, El-Sayed MA (2009) Surface-enhanced Raman scattering enhancement by aggregated silver nanocube monolayers assembled by the Langmuir-Blodgett technique at different surface pressures. J Phys Chem C 113(14):5493–5501. https://doi.org/10.1021/jp900648r

34. Wurtz GA, Evans PR, Hendren W, Atkinson HR, Dickson W, Pollard RJ, Zayats AV, Harrison W, Bower C (2007) Molecular plasmonics with tunable exciton-plasmon coupling strength in J-aggregate hybridized Au nanorod assemblies. Nano Lett 7(5):1297–1303. https://doi.org/10.1021/nl070284m

35. Krivenkov V, Goncharov S, Nabiev I, Rakovich YP (2019) Induced transparency in plasmon-exciton nanostructures for sensing applications. Laser Photonics Rev 13:1800176. https://doi.org/10.1002/lpor.201800176

36. Chen M, Shao L, Woo KC, Wang J, Lin HQ (2012) Plasmonic-molecular resonance coupling: plasmonic splitting versus energy transfer. J Phys Chem C 116(26):14088–14095. https://doi.org/10.1021/jp303560s

37. Kang ESH, Chen S, Sardar S, Tordera D, Armakavicius N, Darakchieva V, Shegai T, Jonsson MP (2018) Strong plasmon-exciton coupling with directional absorption features in optically thin hybrid nanohole metasurfaces. ACS Photonics 5(10):4046–4055. https://doi.org/10.1021/acsphotonics.8b00679

38. Zengin G, Geshneidtner T, Verre R, Shao L, Antosiewicz TJ, Moth-Poulsen K, Kall M, Shegai T (2016) Evaluating conditions for strong coupling between nanoparticle plasmons and organic dyes using scattering and absorption spectroscopy. J Phys Chem C 120(37):20588–20596. https://doi.org/10.1021/acs.jpcc.6b00219

Publisher's Note